Available online at www.sciencedirect.com
ScienceDirect
Bioorganic & Medicinal Chemistry 15 (2007) 4609–4617
Bioorganic & Medicinal Chemistry

2D QSAR studies on thyroid hormone receptor ligands

Napoleão F. Valadares,[a,*] Marcelo S. Castilho,[b] Igor Polikarpov[a] and Richard C. Garratt[a]

[a]*Departamento de Física e Informática, Instituto de Física de São Carlos, Universidade de São Paulo, Av. Trabalhador São-carlense 400, 13560-970 São Carlos-SP, Brazil*
[b]*Laboratório de Bioinformática e Modelagem Molecular, Faculdade de Farmácia, Universidade Federal da Bahia, Campus Universitário de Ondina, 40170-290 Salvador-BA, Brazil*

Received 27 January 2007; revised 27 March 2007; accepted 4 April 2007
Available online 10 April 2007

Abstract—2D QSAR studies were carried out for a series of 55 ligands for the Thyroid receptors, TRα and TRβ. Significant cross-validated correlation coefficients ($q^2 = 0.781$ (TRα) and 0.693 (TRβ)) were obtained. The models' predictive abilities were proved more valuable than the classical 2D-QSAR, and were further investigated by means of an external test set of 13 compounds. The predicted values are in good agreement with experimental values, suggesting that the models could be useful in the design of novel, more potent TR ligands. Contribution map analysis identified a number of positions that are promising for the development of receptor isoform specific ligands.

1. Introduction

Members of the nuclear receptor superfamily, thyroid hormone receptors (TRs), are ligand-activated transcriptional factors that are involved in cell differentiation, growth, and homeostasis.[1,2] Currently, thyroid hormone mimetics are used for the treatment of hypothyroidism, although additional therapeutic indication in the reduction of hyperlipidemia and in weight loss could be anticipated, if the adverse effects of thyroid hormone, namely cardiac toxicity, could be reduced or eliminated.[3,4] As a major contribution to reach this goal, the main isoforms of the thyroid receptor (TRα1 and TRβ1) have been extensively characterized[5] and their differential expression in human organs recognized as a key factor for drug development.[3] Indeed, recent research suggests that specific ligands for TRα1 or TRβ1 may elicit distinct pharmacological effects.[3,4,6]

TRα1 is located mainly in heart tissue and accounts for cardiac responses to the levels of T3, such as tachycardia. On the other hand, the majority of the effects of thyroid hormones on the liver, including its effects on cholesterol metabolism, are mediated by TRβ1.[3] Accordingly, there is growing evidence that selective TRβ1 agonists may be useful in the treatment of obesity and hypercholesterolemia.[3,4,6]

This fact prompted Karo Bio in collaboration with Brystol-Myers Squibb to undertake a structure-based ligand design approach toward TRβ1 selective activation.[7–11] Although their strategy has provided sub-nanomolar ligands of TRβ1, as far as we are aware, no quantitative structure–activity study on available compounds has been conducted.

In the present study, we have collected IC_{50} values for a large series of TRα and TRβ ligands and, employing both classical and hologram QSAR methods, used the data to create QSAR models which show substantial predictive power. Hologram QSAR (HQSAR) is a 2D-QSAR approach that avoids not only the calculation and selection of physicochemical descriptors, but also the need for molecular alignment and conformer generation required for more sophisticated 3D-QSAR methods.[12]

2. Experimental

2.1. Data set

The data set of 68 compounds used for the QSAR studies was selected from the literature.[7–11] The chemical

Keywords: Thyroid Hormone; HQSAR; Selectivity; Contribution Maps.
* Corresponding author. Tel.: +55 16 3373 9874; e-mail: napo@if.sc.usp.br

0968-0896/$ - see front matter © 2007 Elsevier Ltd. All rights reserved.
doi:10.1016/j.bmc.2007.04.015

structures and biological properties for the complete set of compounds are listed in Table 1.

The IC_{50} values were determined under standardized experimental conditions through a binding assay as described by Ye.[7] The fact that all biological data were acquired by the same group (Karo Bio) renders these data comparable in terms of reproducibility, a fundamental requirement for successful QSAR analysis. Collected IC_{50} values vary from 26 μM to 0.1 nM for the TRα isoform and from 5.7 μM to 0.019 nM for TRβ. These data were converted into the corresponding pIC_{50} ($-\log IC_{50}$) and then used in the QSAR studies. The pIC_{50} values are normally distributed across the range of values. Accordingly, the IC_{50} values were considered comparable and thus merged into our study. Taken together, these facts indicate that the data set is suitable for QSAR models development (Fig. 1). However, most compounds in the data set are selective toward TRβ at least to some extent, as can be seen in Figure 2.

Cluster analysis using Euclidean distances and the complete linkage method, carried out in the PIROUETTE software (Infometrix), reveals that these thyroid receptor ligands can be grouped into four distinct clusters for both thyroid isoforms. Members from each cluster were then randomly assigned to the training set (compounds **1**–**55**, Table 1) and test set (compounds **56**–**68**, Table 1). This analysis was not able to provide further insight into chemical or biological features that are important for thyroid binding, however it guarantees that both training and test sets represent the structural diversity and cover the whole data set potency space.

The 3D structures of the thyromimetics were constructed using CONCORD and standard geometric parameters of the molecular modeling software package SYBYL 7.2. Each molecule's single optimized conformation was energy-minimized employing the atom-centered partial charge MNDO-ESP calculations implemented in MOPAC 6.0.

2.2. Descriptor calculation and selection

2D descriptors were calculated using DRAGON (Talete srl) software and subjected to the following selection criteria: Descriptors possessing constant values as well as those with poor correlation to the biological property ($r^2 < 0.10$) were discarded. This strategy provided 575 descriptors that were employed in classical QSAR modeling.

2.3. Classical QSAR studies

The BUILDQSAR software was employed to systematically search for models of up to four variables that gave rise to multiple linear regression (MLR) models with $r^2 > 0.65$. All descriptors present in the MLR models were pooled together, autoscaled, and used for PLS analysis using the PIROUETTE software.

PLS models were selected according to the leave-one-out cross-validated r^2 (q^2) value, using no more than four principal components. Visual analysis of the PLS loadings guided the selection of the most important descriptors during model development.

2.4. HQSAR modeling

Statistical HQSAR modeling was carried out as previously described.[13,14] The concept behind this technique is the use of molecular substructures expressed as a binary pattern, or fingerprint, as descriptors in the QSAR models. Accordingly, each molecule in the data set is broken down into several unique structural fragments, which are arranged to form a molecular hologram. HQSAR encodes all possible molecular fragments (i.e., linear, branched, and overlapping).[15] Thus, this methodology transforms the chemical representation of a molecule into its corresponding molecular hologram, regardless of 3D information (e.g., 3D structure, putative binding conformations, and molecular alignment). HQSAR models can be affected by a number of parameters concerning hologram generation: hologram length (HL), fragment size, and fragment distinction.[13–15] Several combinations of fragment distinction were considered during the QSAR modeling runs. Holograms were generated using 7 distinct fragment sizes over the 12 default series of hologram lengths (53, 59, 61, 71, 83, 97, 151, 199, 257, 307, 353, and 401 bins). All models generated in our studies were investigated using the full cross-validated r^2 (q^2) Partial Least Squares (PLS) Leave-One-Out (LOO) method. The predictive ability of the models was assessed by their q^2 values and further, in order to evaluate the predictive ability of the best model attained, an external validation method was employed.

3. Results and discussion

An important step in classical QSAR modeling is the selection of appropriate descriptors that are correlated to biological activity. In this work, we employed 2D topological descriptors available in DRAGON 5.4. These theoretical descriptors account for molecular size, shape, and branching information of molecules through graph theoretical invariants.[16] Additional information about charge, polarizability, etc. can be obtained using appropriate weighting.[17] Due to the large number of descriptors available, they were selected based on their correlation to biological activity and capability of producing MLR models with up to four descriptors with at least moderate correlation ($r^2 > 0.65$). This strategy had two goals: to build initial QSAR models that could shed light on structural features important for TR binding, and to select a subset of the most correlated descriptors that could be further explored in QSAR model development. The best models show moderate correlation for both TRα ($r^2 = 0.74$) and TRβ ($r^2 = 0.66$). However, the models can be interchanged with only modest impact on the statistics, suggesting that the subtle chemical features that differentiate TRα from TRβ ligands are not well represented. This scenario could be the result of an incomplete description of the binding event by the selected descriptors. Therefore, in order to develop more

Table 1. Chemical structures of the TRα and TRβ ligands used for 2D-QSAR studies[a]

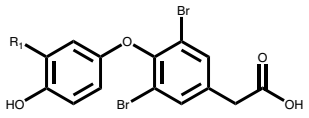

I

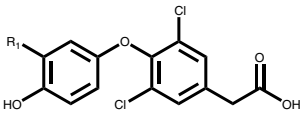

II

Training set compounds

Cpd	Scafold	R_1	TRα pIC_{50}	TRβ pIC_{50}	Cpd	Scafold	R_1	TRα pIC_{50}	TRβ pIC_{50}	Cpd	Scaffold	R_1	TRα pIC_{50}	TRβ pIC_{50}
1	II	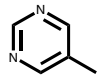	6.57	7.17	**2**	II	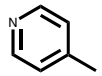	6.84	6.91	**3**	I	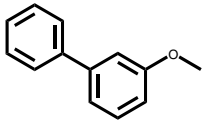	6.30	7.22
4	II		6.25	7.55	**5**	II	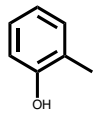	5.98	7.30	**6**	I	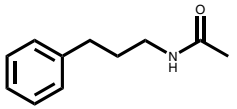	6.69	8.17
7	II		7.60	8.96	**8**	II	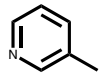	6.09	7.39	**9**	I	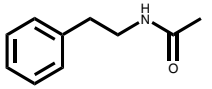	7.82	9.21
10	II	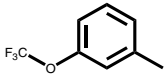	7.00	8.47	**11**	II	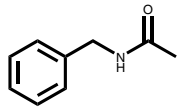	6.90	8.46	**12**	I	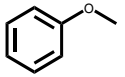	6.91	8.22
13	II	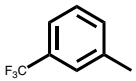	7.40	9.07	**14**	I	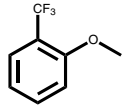	6.61	8.12	**15**	I	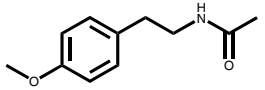	6.64	7.43
16	II	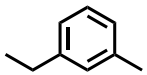	7.89	9.70	**17**	I	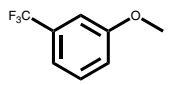	7.30	8.96	**18**	I	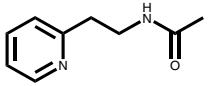	5.94	7.17
19	II	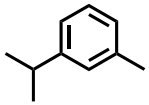	6.91	8.40	**20**	I	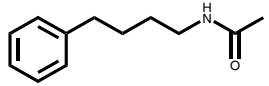	6.55	7.74	**21**	I	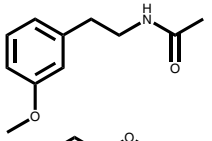	7.03	8.31
22	II	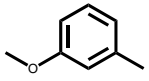	6.53	7.96	**23**	I		8.81	10.02	**24**	I	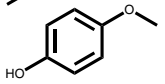	6.62	8.22

(*continued on next page*)

Table 1 (*continued*)

Training set compounds

Cpd	Scafold	R_1	TRα pIC_{50}	TRβ pIC_{50}	Cpd	Scafold	R_1	TRα pIC_{50}	TRβ pIC_{50}	Cpd	Scaffold	R_1	TRα pIC_{50}	TRβ pIC_{50}
25	I	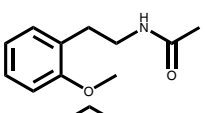	7.02	8.07	**26**	I	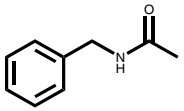	7.07	8.38	**27**	I	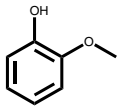	5.83	7.08
28	I	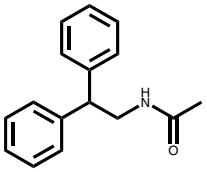	7.74	9.33	**29**	II		5.82	6.86	**30**	I	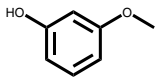	6.26	7.33
31	II	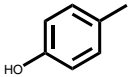	6.07	7.06										

Cpd		TRα pIC_{50}	TRβ pIC_{50}	Cpd		TRα pIC_{50}	TRβ pIC_{50}	Cpd		TRα pIC_{50}	TRβ pIC_{50}
32	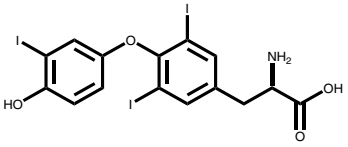	9.62	9.58	**33**	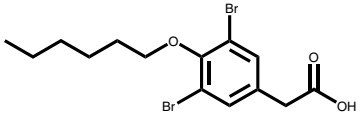	5.28	5.82	**34**	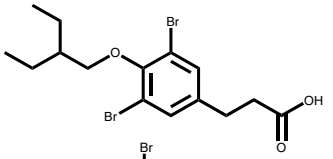	5.80	6.09
35	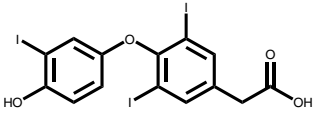	9.85	10.39	**36**	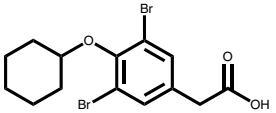	5.57	6.11	**37**	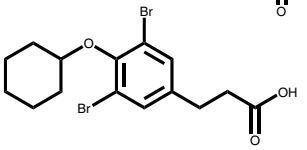	6.34	6.72
38	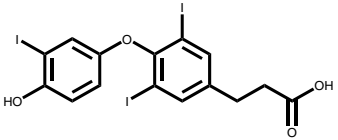	10.39	10.72	**39**	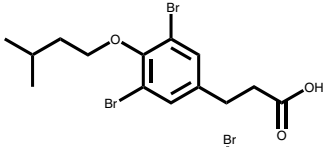	5.36	5.74	**40**	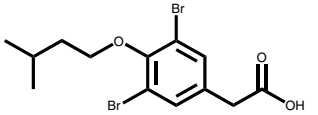	4.89	5.74
41	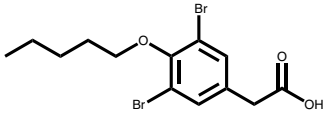	4.70	5.24	**42**	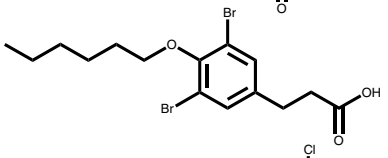	5.96	6.44	**43**	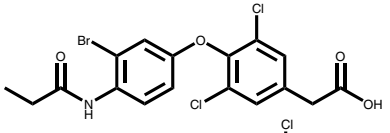	5.48	6.85
44	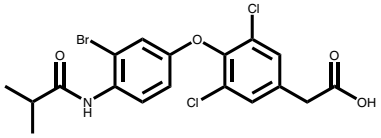	6.20	7.74	**45**	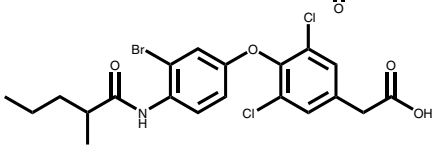	5.89	7.33	**46**	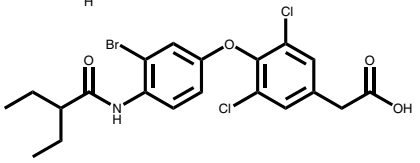	6.21	7.80

47	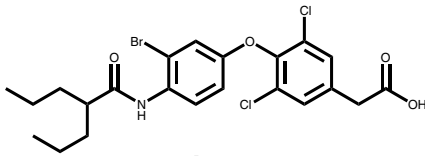	5.92	7.35	**48**	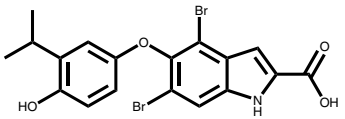	8.60	9.55	**49**	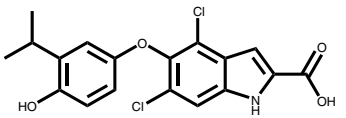	8.85	10.22
50	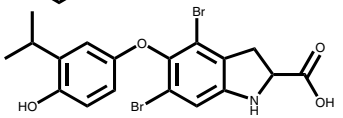	7.42	8.07	**51**	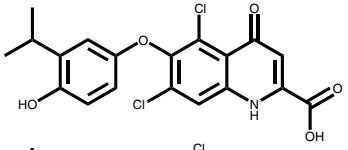	5.46	7.82	**52**	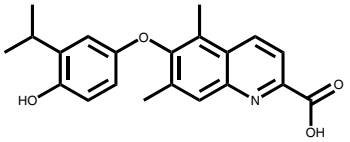	6.70	7.82
53	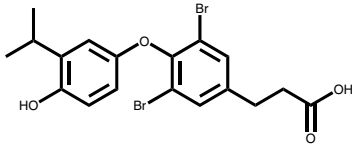	10.00	10.60	**54**	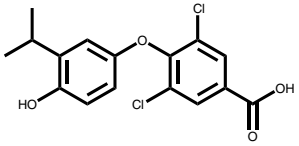	6.89	7.68	**55**	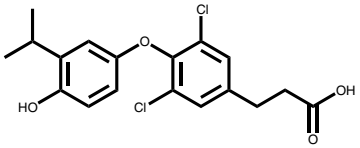	9.12	9.82

Test set compounds

56	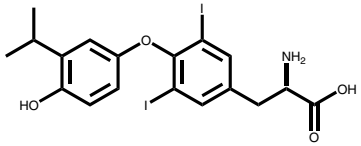	9.85	9.96	**57**	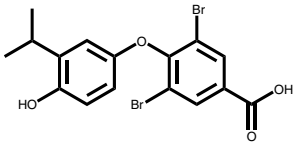	8.01	8.68	**58**	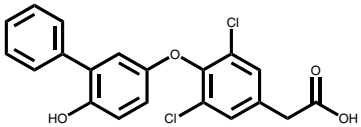	6.89	8.54
59	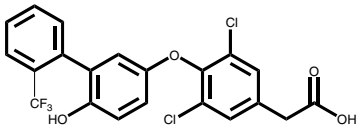	7.74	8.49	**60**	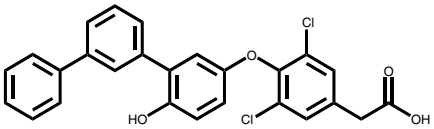	6.34	7.68	**61**	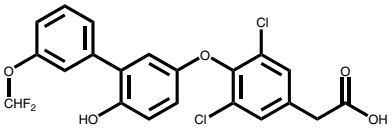	7.52	9.11
62	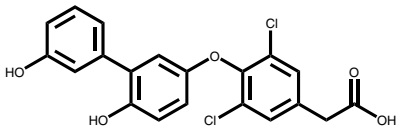	5.93	7.12	**63**	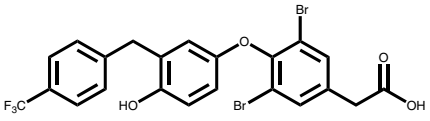	6.47	8.02	**64**	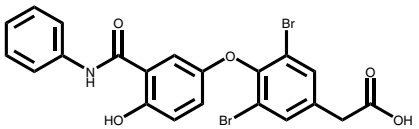	6.37	7.45
65	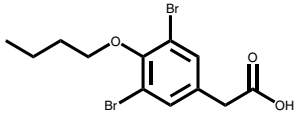	4.58	5.72	**66**	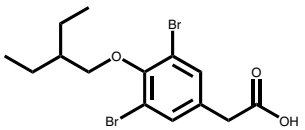	5.16	6.10	**67**	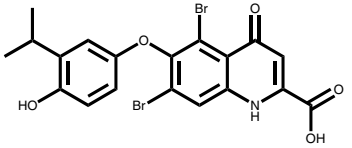	6.60	7.29
68	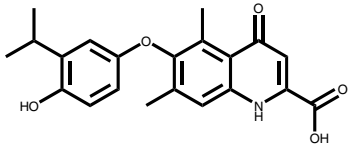	6.21	6.62								

[a] cpd, compound, $pIC_{50} = -\log(IC_{50})$.

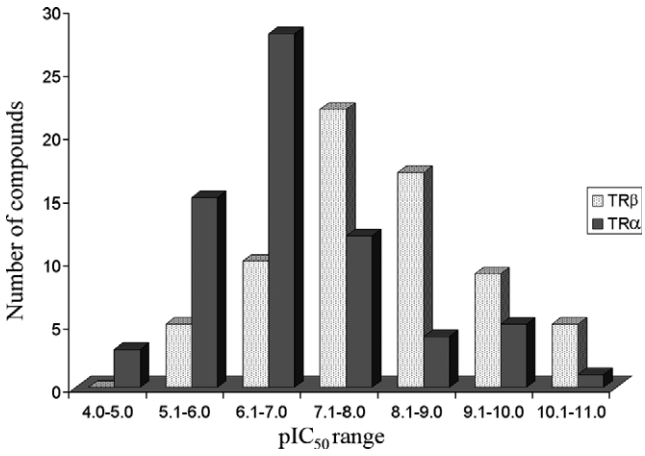

Figure 1. pIC_{50} values distribution for TRα and TRβ inhibitors.

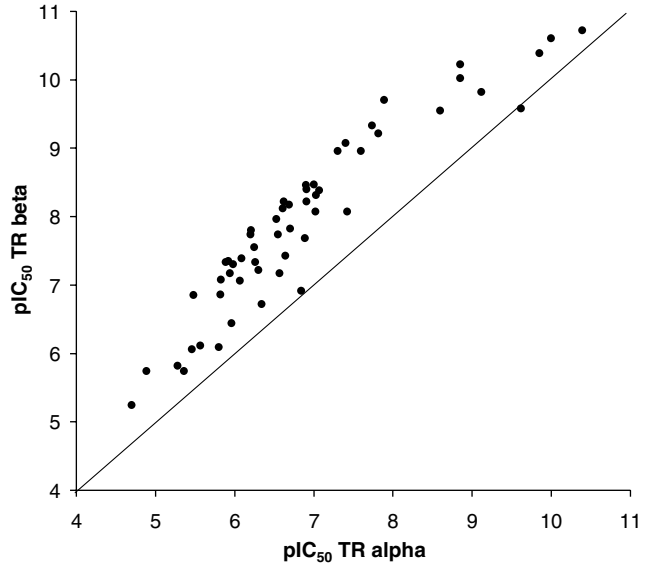

Figure 2. pIC_{50} values for the TRα and TRβ ligands in the data set. Compounds above the line are selective toward TRβ and the compounds below the line are selective toward TRα.

robust models, all descriptors from the MLR models with $r^2 > 0.65$ (4 for TRα and 1 for TRβ) (Table 2) were pooled together, autoscaled, and PLS analysis was carried out with the PIROUETTE software. However, no further model improvement was attained.

As an alternative approach, we resorted to the Hologram QSAR (HQSAR) strategy. In our studies SYBYL 7.2 was used to investigate the influence of the three parameters: fragment distinction, fragment size, and hologram length (HL), on the statistical values of our models. Each model has its own fragment distinction formed by a combination of two or more of the following parameters: atoms (A), bonds (B), connections (C), hydrogen atoms (H), chirality (Ch), and donor and acceptor (DA). Each of these parameters modifies the way the fragments are distinguished, for instance the chirality parameter allows cis double bonds to be distinguished from their trans counterparts, and R-enantiomers to be distinguished from S at all chiral centers.

As can be seen in Tables 3 and 4, the best statistical results among all models were obtained for model 14A for TRα ($q^2 = 0.77$, and $r^2 = 0.90$, with four components) and 14B for TRβ ($q^2 = 0.69$, and $r^2 = 0.87$, with three components). Both models were derived using atoms, bonds, connections, and donor and acceptor as fragment distinction. The use of additional fragment distinctions decreases the quality of the models as measured by the statistical parameters in Table. 3 and 4. For

Table 3. TRα HQSAR analyses for various fragment distinctions on the key statistical parameters using the default fragment size (4–7)

Model	Fragment distinction	q^2	r^2	SEE	HL	N
1A	A/B	0.53	0.85	0.53	307	4
2A	A/B/C	0.69	0.86	0.50	353	4
3A	A/B/C/H	0.63	0.83	0.55	307	4
4A	A/B/C/H/Ch	0.62	0.83	0.56	307	4
5A	A/B/C/H/Ch/DA	0.63	0.84	0.54	307	4
6A	A/B/C/H/DA	0.64	0.82	0.57	151	4
7A	A/B/H	0.63	0.86	0.50	353	4
8A	A/B/H/Ch	0.59	0.81	0.59	401	4
9A	A/B/C/Ch	0.68	0.85	0.53	151	4
10A	A/C/DA	0.64	0.84	0.54	257	4
11A	A/C/H/DA	0.62	0.84	0.53	401	4
12A	A/B/C/Ch/DA	0.75	0.89	0.44	353	4
13A	A/B/DA	0.67	0.87	0.49	307	4
14A	A/B/C/DA	0.77	0.90	0.41	353	4
15A	A/C/Ch/DA	0.63	0.84	0.53	257	4

Table 2. Descriptors employed in classical QSAR model development, via PLS analysis

BEHe3	Highest eigenvalue no. 3 of Burden matrix weighted by atomic Sanderson electronegativity
BEHm8	Highest eigenvalue no. 8 of Burden matrix weighted by atomic mass
BEHv3	Highest eigenvalue no. 3 of Burden matrix weighted by atomic van der Waals volume
BEHp3	Highest eigenvalue no. 3 of Burden matrix weighted by atomic polarizability
BEHp2	Highest eigenvalue no. 2 of Burden matrix weighted by atomic polarizability
nRCONHR	Number of aliphatic secondary amides
ATS7m	Broto-Moreau autocorrelation of a topological structure –lag 7 weighted by atomic mass
MATS2e	Moran autocorrelation –lag 2 weighted by atomic Sanderson electronegativity
GATS3v	Geary autocorrelation –lag 2 weighted by atomic van der Waals volume
GATS2e	Geary autocorrelation –lag 2 weighted by atomic Sanderson electronegativity
GATS8p	Geary autocorrelation –lag 8 weighted by atomic polarizability
EEig06x	Eigenvalue 06 from edge adjacency matrix weighted by edge degrees
EEig07x	Eigenvalue 07 from edge adjacency matrix weighted by edge degrees
EEig09d	Eigenvalue 09 from edge adjacency matrix weighted by dipole moments

Table 4. TRβ HQSAR analyses for various fragment distinctions on the key statistical parameters using the default fragment size (4–7)

Model	Fragment distinction	q^2	r^2	SEE	HL	N
1B	A/B	0.42	0.76	0.67	151	3
2B	A/B/C	0.58	0.80	0.61	151	4
3B	A/B/C/H	0.54	0.77	0.66	401	4
4B	A/B/C/H/Ch	0.53	0.81	0.61	307	4
5B	A/B/C/H/Ch/DA	0.59	0.78	0.65	59	4
6B	A/B/C/H/DA	0.60	0.79	0.63	307	3
7B	A/B/H	0.49	0.75	0.69	401	4
8B	A/B/H/Ch	0.50	0.76	0.67	401	4
9B	A/B/C/Ch	0.57	0.80	0.61	151	4
10B	A/C/D	0.52	0.73	0.71	71	3
11B	A/C/H/DA	0.53	0.78	0.64	401	4
12B	A/B/C/Ch/DA	0.68	0.85	0.52	353	3
13B	A/B/DA	0.65	0.85	0.53	307	4
14B	A/B/C/DA	0.69	0.87	0.50	353	3
15B	A/C/Ch/DA	0.51	0.80	0.61	257	4

instance, adding chirality to the atom distinction does not improve the model (compare 12A with 14A and 12B with 14B). This outcome is not unexpected since most compounds in our data set are not chiral. Furthermore, our results confirm previous studies which suggest that 'donor and acceptor' fragment generation should not be used simultaneously with hydrogen atoms[15,18] due to the substantial increase in the number of fragments generated when both of these options are considered in the model construction.

On the other hand, considering donor and acceptor atoms in fragment distinction dramatically improved the model (compare 2A and 14A or 2B and 14B). This result is in good agreement with crystallographic data, which show that hydrogen bonding plays an important role for TR ligand binding.[11,19]

The influence of different fragment sizes over the statistical parameters was further investigated for HQSAR models 14A and 14B. Fragment size parameters control the minimum and maximum length of fragments to be included in the hologram fingerprint. The HQSAR results for different fragment sizes are summarized in Table 5. The results show that variation of the fragment size (5–8) provided an improvement in the HQSAR model for TRα, whereas the default fragment size (4–7) led to the best statistical results for TRβ (highlighted in Table 5).

The leave-one-out procedure used in our studies might produce high q^2 values which do not necessarily give a suitable representation of the real predictive power of the models for TR ligands.[20] Thus, we employed a leave-many-out procedure with either 15, 10 or 5 groups of compounds. The results are not significantly different from those obtained using the LOO approach for both TR isoforms. Finally, the predictive power of the best HQSAR models was assessed by predicting pIC_{50} values for 13 test set molecules (compounds **56**–**68**, Table 1), which were not included in the HQSAR model development. The results are listed in Table 6 and the experimental versus predicted activities of both training set and test set are depicted in Figures 3 and 4.

Table 5. Influence of fragment sizes on the statistical parameters using the best fragment distinction (atoms, bonds, connections, donor, and acceptor)

Model	Fragment size/TR isoform	q^2		r^2		SEE		HL		N	
		TRα	TRβ	TRα	TRβ	TRα	TRβ	TRα	TRβ	TRα	TRβ
16 A/B	2–5	0.72	0.64	0.85	0.82	0.53	0.59	61	61	4	4
17 A/B	3–6	0.76	0.64	0.87	0.81	0.47	0.59	151	151	4	3
18 A/B	4–7	0.77	0.69	0.90	0.87	0.41	0.50	353	353	4	3
19 A/B	5–8	0.78	0.68	0.90	0.86	0.43	0.51	401	401	4	4
20 A/B	6–9	0.76	0.66	0.89	0.86	0.44	0.52	401	401	4	4
21 A/B	7–10	0.74	0.65	0.88	0.87	0.47	0.49	353	401	4	4
22 A/B	8–11	0.72	0.60	0.88	0.84	0.47	0.55	353	353	4	4

Table 6. Experimental and predicted values of pIC_{50} for the test set compounds, according to models 18B and 19A

Test set pIC_{50}	Experimental		Predicted		Residual	
TR Isoform	TRα	TRβ	TRα	TRβ	TRα	TRβ
3	9.85	9.96	9.88	10.80	−0.03	−0.84
6	8.01	8.68	8.45	8.88	−0.44	−0.20
11	6.89	8.54	6.50	7.79	0.39	0.75
12	7.74	8.49	7.36	8.78	0.38	−0.29
17	6.34	7.68	6.31	7.82	0.03	−0.14
19	7.52	9.11	6.97	8.41	0.55	0.70
22	5.93	7.12	6.37	7.62	−0.44	−0.50
33	6.47	8.02	6.94	8.49	−0.47	−0.47
38	6.37	7.45	6.66	7.52	−0.29	−0.07
51	4.58	5.72	5.14	5.77	−0.56	−0.05
55	5.16	6.10	4.98	5.51	0.18	0.59
70	6.60	7.29	5.79	7.09	0.81	0.20
72	6.21	6.62	6.71	7.53	−0.50	−0.91

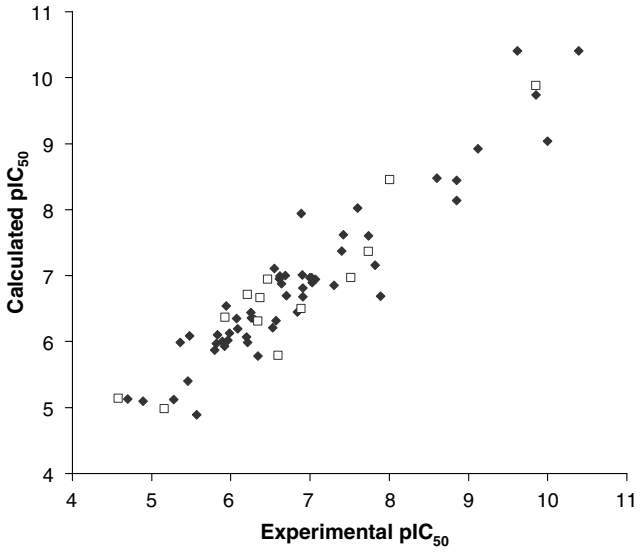

Figure 3. Calculated versus experimental pIC_{50} values for TRα ligands. The diamonds refer to the training set and the open squares to the test set.

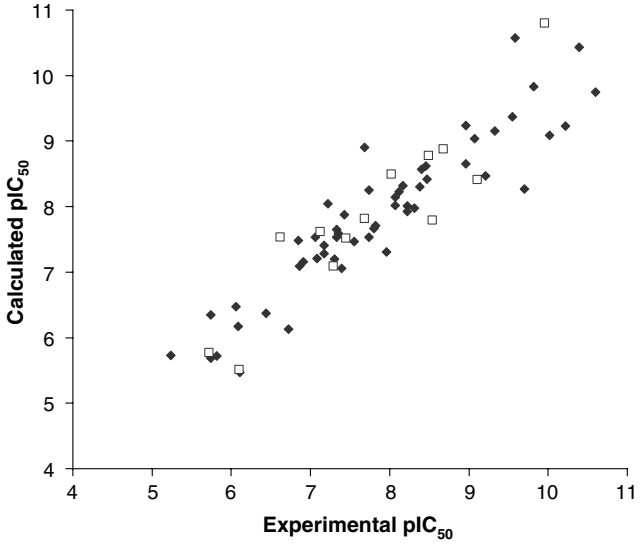

Figure 4. Calculated versus experimental pIC_{50} values for TRβ ligands. The diamonds refer to the training set and the open squares to the test set.

The good agreement between experimental and predicted values for the test set compounds indicates the reliability of the constructed HQSAR models, especially for TRα ($r^2 = 0.895$, SEE = 0.433). The residual values are low (less than 1 log unit), indicating that the obtained HQSAR models are reliable and can be used to predict the biological activity of novel compounds within this structural class. In addition to predict the activities of untested molecules, QSAR models shed some light on structural and chemical features that are directly related to biological activity.

HQSAR provides information about molecular fragments with positive and/or negative influence on

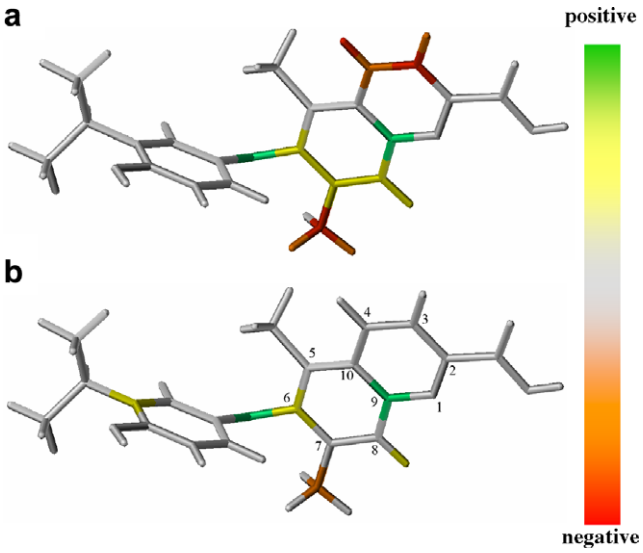

Figure 5. Contribution maps for ligand 52 according to the TRα (a) and TRβ (b) HQSAR model. Atoms are colored according to their contribution to TR binding.

the biological activity. The individual atomic contributions to the biological activity can be visualized through the contribution maps colored according to such contributions. Figure 5 displays the contribution map of compound **52**, which has been synthesized by Collazo and coworkers aiming at exploring the binding site volume unoccupied by previous ligands.[11]

According to the HQSAR model, positions 3 and 4 on the quinoline ring have strong negative contributions for TRα and little effect on TRβ binding. This observation might be associated with steric hindrance of the ligand within the TRα binding site. This hypothesis is supported by the fact that the smaller indole derivative **49** has a hundred fold greater affinity than **52**. This result indicates that flexibility in this ligand moiety is important for TRα binding, but has little effect on its binding to TRβ, and this information might be valuable for the design of compounds selective toward the TRβ isoform.

A second interesting feature highlighted by the contribution maps is the different colors of the substituents at positions 5 and 7. This result may be linked to induced fit upon ligand binding. Once again, TR flexibility seems to be responsible for this result, whereas polarizability and higher electronegativity of bromine or iodine in these positions make them optimal for affinity and stability,[21] smaller chemical moieties in the positions 5 and 7 might be important for TR isoform selectivity. However, as the data set does not explore the chemical space around these positions, it would be worthwhile to synthesize and test ligands with different substituents on these positions to further investigate this result.

4. Conclusion

QSAR models with reliable predictive power for both TRα and TRβ have been successfully generated. All

models presented here were derived using the same training and test sets for all QSAR analyses. The good correlation between experimental and predicted bioactivities for 13 compounds in the test set further highlights the reliability of the constructed HQSAR models. The model for TRβ was slightly less robust, which may be in part due to the greater potency range of the ligands in the data set.

These models which provide information about the importance of specific atomic positions should be complementary to our ongoing research on thyroid hormone receptors, that is aimed at using virtual screening and structure based design to develop selective TRβ ligands.

Acknowledgment

This work was supported by the Fundação de Amparo à Pesquisa do Estado de São Paulo (FAPESP) Grant 02/14205-9, Fundação de Amparo à Pesquisa do Estado da Bahia (FAPESB) Grant 2024/2005 and Conselho Nacional de Desenvolvimento Cientifico e Tecnológico (CNPq) Grant 42.120/2005-0.

Supplementary data

The molecular structures used in this study can be found in the online version. Supplementary data associated with this article can be found, in the online version, at doi:10.1016/j.bmc.2007.04.015.

References and notes

1. Yen, P. M. *Physiol. Rev.* **2001**, *81*, 1097.
2. Grover, G. J.; Malm, J. *Drug Discov. Today: Ther. Strateg.* **2005**, *2*, 137.
3. Yoshihara, H. A. I.; Apriletti, J. W.; Baxter, J. D.; Scanlan, T. S. *J. Med. Chem.* **2003**, *46*, 3152.
4. Chiellini, G.; Nguyen, N. H.; Apriletti, J. W.; Baxter, J. D.; Scanlan, T. S. *Bioorg. Med. Chem.* **2002**, *10*, 333.
5. Lazar, M. A. *Endocr. Rev.* **1993**, *14*, 184.
6. Borngraeber, S.; Budny, M. J.; Chiellini, G.; Cunha-Lima, S. T.; Togashi, M.; Webb, P.; Baxter, J. D.; Scanlan, T. S.; Fletterick, R. J. *Proc. Natl. Acad. Sci. U.S.A.* **2003**, *100*, 15358.
7. Ye, L.; Li, Y.-L.; Mellstrom, K.; Bladh, L.-G.; Koehler, K.; Garg, N.; Garcia Collazo, A. M.; Litten, C.; Husman, B.; Persson, K.; Ljunggren, J.; Grover, G.; Sleph, P. G.; George, R.; Malm, J. *J. Med. Chem.* **2003**, *46*, 1580.
8. Hangeland, J. J.; Doweyko, A. M.; Dejneka, T.; Friends, T. J.; Devasthale, P.; Mellstrom, M.; Sandberg, J.; Grynfarb, M.; Sack, J. S.; Einspahr, H.; Farnegardh, M.; Husman, B.; Ljunggren, J.; Koehler, K.; Sheppard, C.; Malm, J.; Ryono, D. E. *Bioorg. Med. Chem. Lett.* **2004**, *14*, 3549.
9. Hedfors, A.; Appelqvist, T.; Carlsson, B.; Bladh, L.-B.; Litten, C.; Agback, P.; Grynfarb, M.; Koehler, K. F.; Malm, J. *J. Med. Chem.* **2005**, *48*, 3114.
10. Li, Y. L.; Litten, C.; Koehler, K. F.; Mellstrom, K.; Garg, N.; Garcia Collazo, A. M.; Farnegard, M.; Grynfarb, M.; Husman, B.; Sandberg, J.; Malm, J. *Bioorg. Med. Chem. Lett.* **2006**, *16*, 884–886.
11. Garcia Collazo, A. M.; Koehler, K. F.; Garg, N.; Farnegardh, M.; Husman, B.; Ye, L.; Ljunggren, J.; Mellstrom, K.; Sandberg, J.; Grynfarb, M.; Ahola, H.; Malm, J. *Bioorg. Med. Chem. Lett.* **2006**, *16*, 1240.
12. Sutherland, J. J.; O'Brien, L. A.; Weaver, D. F. *J. Med. Chem.* **2004**, *47*, 5541–5554.
13. Castilho, M. S.; Postigo, M. P.; de Paula, C. B.; Montanari, C. A.; Oliva, G.; Andricopulo, A. D. *Bioorg. Med. Chem.* **2006**, *14*, 516–527.
14. Castilho, M. S.; Guido, R. V. C.; Andricopulo, A. D. *Lett. Drug. Des. Discov.* **2007**, *4*, 106–113.
15. HQSARTM Manual, SYBYL 6.9.2, Tripos, St. Louis, MO.
16. Basak, S. C.; Balaban, A. T.; Grunwald, G. D.; Gute, G. D.; Gute, B. D. *J. Chem. Inf. Comput. Sci.* **2000**, *40*, 891–898.
17. Ivanciuc, O.; Ivanciuc, T.; Balaban, A. T. *J. Chem. Inf. Comput. Sci.* **1998**, *38*, 395–401.
18. Honorio, K. M.; Garratt, R. C.; Andricopulo, A. D. *Bioorg. Med. Chem. Lett.* **2005**, *15*, 3119–3125.
19. Wagner, R. L.; Apriletti, J. W.; McGrath, M. E.; West, B. L.; Baxter, J. D.; Fletterick, R. J. *Nature* **1995**, *14*, 690–697.
20. Golbraikh, A.; Tropsha, A. *J. Mol. Graph. Model.* **2002**, *20*, 269–276.
21. Koehler, K.; Gordon, S.; Brandt, P.; Carlsson, B.; Backsbro-Saeidi, A.; Apelqvist, T.; Agback, P.; Grover, G. J.; Nelson, W.; Grynfarb, M.; Farnegardh, M.; Rehnmark, S.; Malm, J. *J. Med. Chem.* **2006**, *49*, 6635.